



JGR Solid Earth

RESEARCH ARTICLE

10.1029/2019JB019047

Key Points:

- Long-period ground motions for Nankai Trough earthquakes are forecasted by assimilation of observed ground motion and numerical simulation
- Speedup of the forecast is achieved by using precalculated Green's functions, ensuring longer lead time before a strong shake occurs
- Recently deployed offshore cable stations significantly improve the accuracy and the lead time of the forecast

Supporting Information:

- Supporting Information S1

Correspondence to:

A. Oba,
atsuki-oba@kke.co.jp

Citation:

Oba, A., Furumura, T., & Maeda, T. (2020). Data assimilation-based early forecasting of long-period ground motions for large earthquakes along the Nankai Trough. *Journal of Geophysical Research: Solid Earth*, 125, e2019JB019047. <https://doi.org/10.1029/2019JB019047>

Received 10 NOV 2019

Accepted 17 MAY 2020

Accepted article online 22 MAY 2020

Data Assimilation-Based Early Forecasting of Long-Period Ground Motions for Large Earthquakes Along the Nankai Trough

Atsuki Oba^{1,2} , Takashi Furumura¹ , and Takuto Maeda³

¹Earthquake Research Institute, The University of Tokyo, Tokyo, Japan, ²Kozo Keikaku Engineering Inc., Tokyo, Japan,

³Graduate School of Science and Technology, Hirosaki University, Aomori, Japan

Abstract Long-period (LP) ground motions with periods of ~2–10 s caused by large earthquakes are strongly amplified in sedimentary basins, posing serious threats to modern cities to cause resonance and damage to skyscrapers, oil storage tanks, long-span bridges, and other structures with long natural periods. Since the LP ground motions are composed of surface waves traveling for longer distances with much slower speeds than body waves, an alert could be issued by detecting the spread of strong ground motion near the source and before large ground motions occur in distant basins. In this study, an early forecasting of LP ground motions is proposed based on data assimilation of observed ground motions obtained by high-density, nationwide seismic networks and a computer simulation of the seismic wave propagation using a high-resolution subsurface structure model. The shaking of the LP ground motions in the distant basins is immediately forecasted by high-speed supercomputers from current data-assimilated wavefield. In addition, the forecasting speed is significantly improved by using Green's functions, representing the wave propagation response from the data assimilation stations to a forecast target site. The effectiveness of this data assimilation-based forecasting of LP ground motions in conjunction with using Green's functions is demonstrated by numerical tests using the observed strong motion records from the 2004 Off Kii Peninsula earthquake in Japan (Mw 7.4) together with synthetic seismograms of anticipated large earthquake scenarios in the Nankai Trough.

1. Introduction

Long-period (LP) ground motions with periods of approximately 2–10 s caused by large earthquakes can travel for large distances without large attenuation owing to their long wavelength, and they are dramatically amplified when traveling into large sedimentary basins. This results in large and lengthy LP ground motions causing resonance and damage in large-scale structures, such as skyscrapers, long-span bridges, and large oil storage tanks with long natural periods.

One of the most well-known disasters owing to the LP ground motions occurred in the ancient lake of Mexico City during the 1985 Michoacan earthquake (Mw 8.0). Though the city was located 400 km away from the epicenter, intense and lengthy ground motions in periods of 2–3 s collapsed multistory buildings owing to resonance (Beck & Hall, 1986). In 2003, Tokachi-Oki, Japan, experienced a Mw 8.0 earthquake whose LP ground motions caused damage to an oil storage tank at Tomakomai in the Yufutsu basin some 200 km away from the epicenter (Koketsu et al., 2009). During the 2004 Off Kii Peninsula earthquake in Japan (Mw 7.4), sloshing damage occurred in an oil storage tank in Tokyo Bay, 300 km away from the epicenter (Hatayama & Zama, 2005).

In southwest Japan, large earthquakes around M 8 have repeatedly occurred in the Nankai Trough (hereafter referred to as Nankai Trough earthquakes) at intervals of ~100–200 years (Ando, 1975). The most recent events were the 1944 Tonankai (M 7.9) and the 1946 Nankai (M 8.0) earthquakes, which occurred on the east and west sides of the Nankai Trough, respectively. According to the long-time forecast from the Headquarters for Earthquake Research Promotion (2018), the next Nankai Trough earthquake is expected to occur in the next 30 years, at a probability of 70–80%. The observed strong motion records of the 1944 Tonankai earthquake demonstrate that large LP ground motions of more than 10 cm and periods between 8 and 10 s occurred in Tokyo for more than several minutes (Furumura et al., 2008; Furumura & Nakamura, 2006). Amplification of the LP surface waves in the accretionary prism along the Nankai

Trough is thought to be a major cause of the large and lengthy LP ground motions, which occurred in Tokyo (e.g., Furumura et al., 2008; Hayakawa et al., 2005). Therefore, it is anticipated that future large Nankai Trough earthquakes might severely impact large-scale buildings in modern, populated cities due to the intense and prolonged shaking of LP ground motions.

In order to mitigate possible disasters caused by large LP ground motions, such as those anticipated for future Nankai Trough earthquakes, an early forecast can be considered in large basins from distant, large earthquakes. Generally, the forecasting of LP ground motions is done based on ground motion prediction equations (GMPEs) obtained empirically using observed strong motion records, as a function of magnitude, fault distance, site amplification factors, and so on (e.g., Dhakal et al., 2015; Ibrahim et al., 2016; Yokota et al., 2011; Yuzawa & Kudo, 2011). Such GMPE-based forecasting was first developed for predicting the peak ground acceleration and shaking intensity of short-period seismic waves less than 1 s period and is extended to much longer period for predicting LP ground motions.

However, the propagation and amplification of the LP ground motions in large basins are significantly influenced by the heterogeneous 3-D subsurface structures along long propagation paths and cause strong focusing and defocusing (e.g., Denolle et al., 2013; Frankel et al., 2018; Furumura & Hayakawa, 2007; Mukai et al., 2018; Wirth et al., 2019). For example, the amplification of the LP ground motions in the Kanto basin was shown to have large variations with respect to the incident angle of the LP surface waves to the basin edge; the amplification was larger for the earthquakes occurring in the north to southwest of Tokyo, whereas it is much weaker for the earthquakes occurring in the northeast (e.g., Furumura, 2014; Uetake, 2017; Yuzawa & Nagumo, 2012). Also, the earthquakes occurring in the Nankai Trough are usually characterized by longer durations of LP ground motions after traversing the accretionary wedge of the Nankai Trough subduction zone (Furumura et al., 2008; Hayakawa et al., 2005). Such effects of 3-D subsurface structure on amplification and elongation of the LP ground motion cannot be adequately evaluated by the GMPEs.

In large earthquakes, the strong ground motions radiate sequentially from multiple strong motion generation areas (SMGAs) as the rupture propagates over the source fault. For example, the source model of the 2011 Tohoku earthquake in Japan (M_w 9.0) was characterized by four or five SMGAs over the large megathrust (Asano & Iwata, 2012; Kawabe & Kamae, 2013; Kurahashi & Irikura, 2013). Also, the source models of the 1944 Tonankai earthquake (M_w 7.9) and the 1946 Nankai earthquake (M_w 8.0) produced by the Cabinet Office of the Disaster Prevention Section (2015) for the modeling of LP ground motions consist of four SMGAs on the large (about 100 km \times 300 km) source faults. Owing to the presence of multiple SMGAs in large faults, it is difficult to forecast the LP ground motions in real time during the propagation of a fault rupture.

To accomplish real-time forecasting of the LP ground motions for large earthquake, an alternative approach was considered, which is not based on the GMPEs but instead on the observed wavefield during the earthquakes, as conducted by Furumura et al. (2019). As the propagation speed of the surface waves that generate LP ground motion is relatively slow, the early forecast of the LP ground motions in distant basins is possible subsequent to detecting large ground motions near the epicenter. This forecast approach of Furumura et al. (2019) is based on data assimilation of the observed ground motions obtained by a dense nationwide network and a high-resolution seismic wave propagation simulation in a 3-D heterogeneous structure. As soon as data assimilation is completed, forecast of the LP ground motions in the future time is done by seismic wave propagation simulations using a high-speed supercomputer in real time from the current data assimilated wavefield.

To achieve a forecast more quickly, this study uses precalculated Green's functions for wave propagation from the data assimilation stations to the forecast target site, instead of performing in situ seismic wave propagation simulations. Such data assimilation-based forecasts (DAFs) using Green's functions were first proposed by Wang et al. (2017) for an early tsunami forecasting (Green's Function-Based Tsunami Data Assimilation, GFTDA), and here, its applicability for seismic waves is examined.

In the following sections, we first examine the effectiveness of the DAF of Furumura et al. (2019) for the forecasting of LP ground motions in large basins such as Tokyo, using observed records of the 2004 Off Kii Peninsula earthquake (M_w 7.4), which occurred in the Nankai Trough. The DAF is then extended through the use of precalculated Green's functions to achieve much faster forecasts. The effectiveness of the DAF using Green's functions (hereafter referred to as the DAF + G) for the early forecasting of LP ground

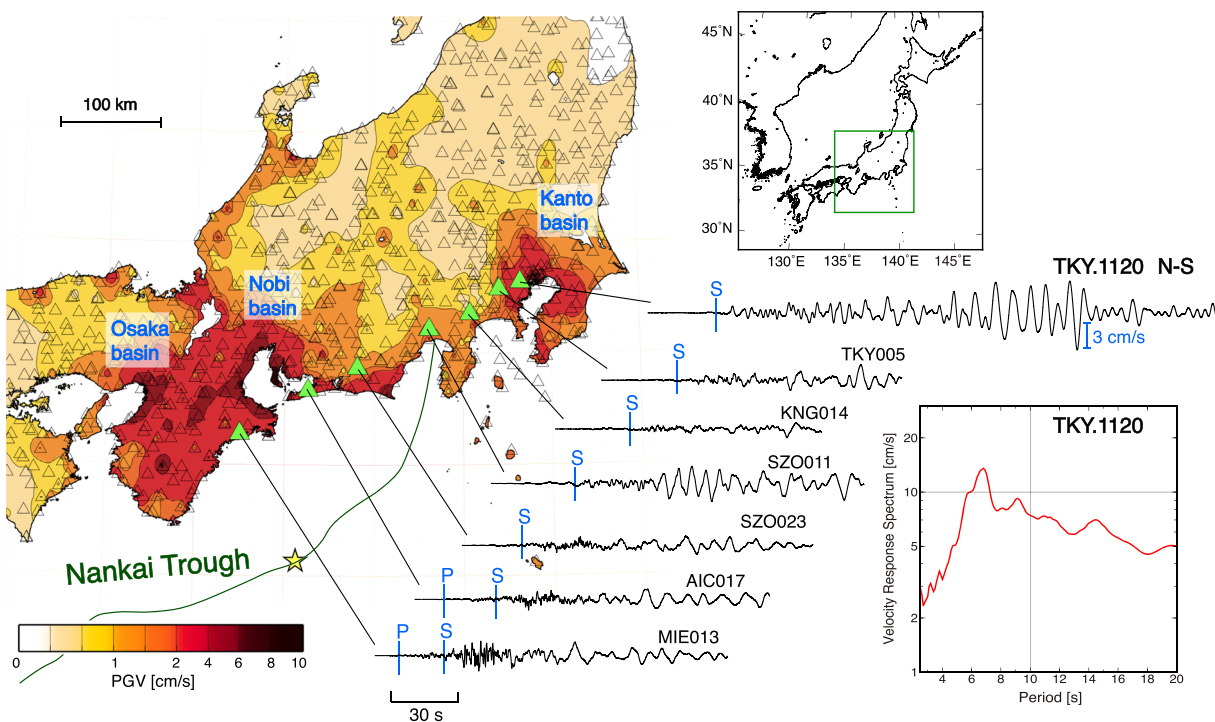


Figure 1. The peak ground velocity (PGV) distribution of the 2004 Off Kii Peninsula, Japan, earthquake of $M_w 7.4$. The LP ground motions of the N-S component ground velocity at seven stations (green triangles) located near the source at Nankai Trough to Tokyo are presented. The velocity response spectrum of horizontal ground motions with a 5% damping at a station in Setagaya, Tokyo (TKY.1120), is presented on the right.

motions is demonstrated through numerical tests using observed records of the 2004 Off Kii Peninsula earthquake and synthetic seismograms for anticipated Nankai Trough earthquake scenarios. The effect of the recently developed offshore ocean-bottom cable stations in the Nankai Trough is also examined on early forecasting.

2. Early Forecasting of LP Ground Motions via Data Assimilation of Observed Ground Motions

2.1. Observed LP Ground Motions of the 2004 Off the Kii Peninsula Earthquake

On 5 September 2004, a large $M_w 7.4$ earthquake occurred in the subducting Philippine Sea plate at a depth of 11 km (hereafter referred to as the 2004 Off Kii Peninsula earthquake) and generated powerful and lengthy LP ground motions in large basins, such as in Osaka, Nobi (Nagoya), and Kanto (Tokyo). Figure 1 presents the distribution of the peak ground velocity (PGV) of the horizontal motions over western-central Japan obtained by the K-NET and KiK-net (Aoi et al., 2011) records from the NIED. An anomalously large PGV of more than 3 cm/s in the Kanto basin, located more than 300 km away from the epicenter, indicates significant amplification of the LP ground motions within the thick sedimentary layers of the Kanto basin (Miyake & Koketsu, 2005; Hayakawa et al., 2005).

Records of the N-S component ground velocity by the K-NET, KiK-net, and SK-net stations, which are located from near the hypocenter to inside the Kanto basin (Figure 1), demonstrate the development of large and long-lasting LP surface waves after traveling for long distances through the Nankai Trough. As the strong motion instruments are recorded by the event trigger system, the LP ground motions are not sufficiently recorded for most of the distant stations owing to low acceleration levels. However, the relatively longer records are obtained at SK-net TKY.1120 station in Setagaya, Tokyo, where the large LP ground motion started about 160 s after the earthquake occurrence time, and strong shaking up to ~ 3 cm/s lasted for more than several hundred seconds. Therefore, we used this station record to examine the results of data assimilation and forecasting experiments. The velocity response spectrum (5% damping) of the horizontal

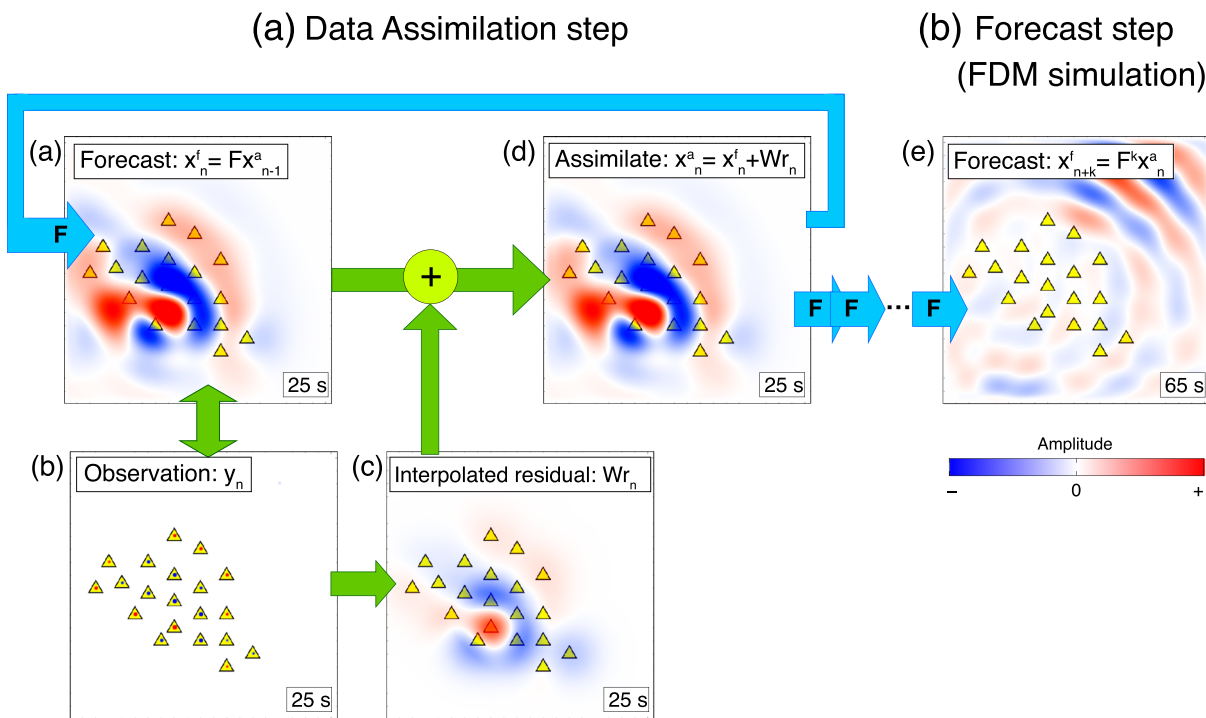


Figure 2. Schematic illustration of the DAF for (a) data assimilation steps and (b) the forecast step of the LP ground motions. (a) The forecasted wavefield at the present time step obtained using 3-D FDM simulation is compared with (b) the observed ground motion at each station (triangle). (c) The residual wavefield over the surface grid points is obtained by spatially interpolating the residuals at each station grid point by applying a weight matrix. (d) Data assimilation is performed by correcting the forecasted wavefield with the interpolated residual data, and the forecasting and assimilation are repeated for a certain time. (e) At a certain time of the data assimilation, the future wavefield is forecasted from the data assimilated wavefield by the 3-D FDM simulations with many time step calculations.

ground motions at TKY.1120 shows a large response of over 10 cm/s in natural period of 7 s. This peak resonant period roughly corresponds to the thickness of the sedimentary layers on the rigid bedrock (Furumura & Hayakawa, 2007), but it is also affected by the source spectrum (i.e., the magnitude of earthquake).

2.2. DAF of the LP Ground Motions

For the early forecasting of LP ground motions from large earthquakes in the Nankai Trough, the DAF developed by Furumura et al. (2019) was applied using nationwide strong motion networks and a high-speed supercomputer.

2.3. Procedure of the DAF

Here, the 3-D (x,y,z) wavefield at the present time $t = n\Delta t$ with the number of time steps n and a time increment of Δt is denoted as a matrix $\mathbf{x}_n = [\mathbf{v}_x(n\Delta t, x, y, z) \mathbf{v}_y(n\Delta t, x, y, z) \mathbf{v}_z(n\Delta t, x, y, z)]$ with the dimension of $G \times 3$, where G denotes a total number of FDM grid points.

The forecasted wavefield at the present time \mathbf{x}_n^f is obtained by the 3-D FDM simulation of the equation of motion from the data assimilated wavefield at the previous time \mathbf{x}_{n-1}^a (Figure 2a):

$$\mathbf{x}_n^f = \mathbf{F} \mathbf{x}_{n-1}^a \quad (1)$$

where \mathbf{F} denotes the wave propagation matrix ($G \times G$), which is solved by the 3-D FDM simulation.

The residual matrix \mathbf{r}_n ($M \times 3$) between the forecasted wavefield \mathbf{x}_n^f and the observed ground motion \mathbf{y}_n ($M \times 3$; Figure 2b) is obtained at M stations by

$$\mathbf{r}_n = \mathbf{y}_n - \mathbf{Hx}_n^f \quad (2)$$

where \mathbf{H} denotes the observation matrix ($M \times G$), which has a component of 1 if the seismic station is available on the FDM grid and a component of 0 otherwise.

Then, data assimilation between the forecasted and the observed wavefield is performed by modifying the forecasted wavefield using the residual wavefield:

$$\mathbf{x}_n^a = \mathbf{x}_n^f + \mathbf{Wr}_n \quad (3)$$

where \mathbf{W} is the weight matrix ($G \times M$) of the optimum interpolation operator (e.g., Kalnay, 2003) that is used to distribute the residual at each station to neighboring grid points (Figure 2c). The \mathbf{W} is calculated so that the covariance between the assimilated and the actual wavefield is minimized; the weight of the residual at the j th station ($j = 1, 2, \dots, M$) with respect to the g th grid ($g = 1, 2, \dots, G$), w_{gj} , is calculated by solving the following equation:

$$\sum_{j=1}^M w_{gj} (\mu_{ij}^b + \delta_{ij} \rho_i \rho_j) = \mu_{gi}^b \quad (4)$$

by considering the correlation of the error between the forecasted wavefield at each pair of FDM grid points and that of stations (μ_{ij}^b ; $i = 1, 2, \dots, M$), and the ratio of the error of the observed waveform (σ_o) relative to that of the forecasted waveform (σ_b) at the i th station ($\rho_i = \sigma_o / \sigma_b$) (see, e.g., Hoshiba & Aoki, 2015; Kalnay, 2003; Maeda et al., 2015, for more detail).

As most of the K-NET and KiK-net stations are located only on the Earth's surface, the data assimilation can be performed only at FDM grid points on the surface, not the entire 3-D grids. However, the reconstruction of the 3-D wavefield from the assimilated wavefield on the surface proceeds steadily as the surface wave propagates for a distance of about a wavelength.

In this study, the estimated wavefield at the present time calculated by repeating forecast (by Equation 1) and assimilation (by Equation 3) is defined as the “assimilated wavefield,” and the wavefield forecasted for a future time (e.g., a few hundred seconds later) without performing assimilation is called the “forecasted wavefield.” The forecasted wavefield is obtained by many 3-D FDM time steps, starting with the current assimilated wavefield (Figure 2e):

$$\mathbf{x}_{n+k}^f = \mathbf{F}^k \mathbf{x}_n^a \quad (5)$$

The time between the forecasting of the wavefield and the arrival of the main LP ground motion is defined as lead time in this study. Obviously, the longer the assimilation lasts for, the closer the forecasted wavefield will be to the actual wavefield; however, there is a trade-off between the accuracy of forecast and the lead time before large ground motion starts. Thus, an optimum assimilation time is chosen considering an acceptable trade-off between the forecast accuracy and the lead time.

2.4. Forecast of LP Ground Motions for the 2004 Off Kii Peninsula Earthquake

In order to examine the feasibility of this DAF approach and its applicability to the LP ground motions of the Nankai Trough earthquakes, a numerical test was conducted using the K-NET and KiK-net records from the 2004 Off Kii Peninsula earthquake (Mw 7.4), which occurred in the Nankai Trough. At present, the K-NET and KiK-net data are not available in real time, but this experiment assumes that the data can be imported to a computer in real time. The N-S and E-W component accelerograms of the 446 K-NET and KiK-net records used in this experiment are presented in section S1 in the supporting information. Some records are missing in the earlier or later part of the LP ground motions owing to the reliance on the event trigger recording system.

The target area of the data assimilation and forecast simulation is 716.8 km × 409.6 km in the horizontal directions and 70 km in depth, which is discretized into grid intervals of 0.2 km in all directions (Figure 3a). The 3-D FDM simulation of seismic wave propagation is conducted using a frequency-independent Qp and Qs model presented by Blanch et al. (1995) with an absorbing boundary as

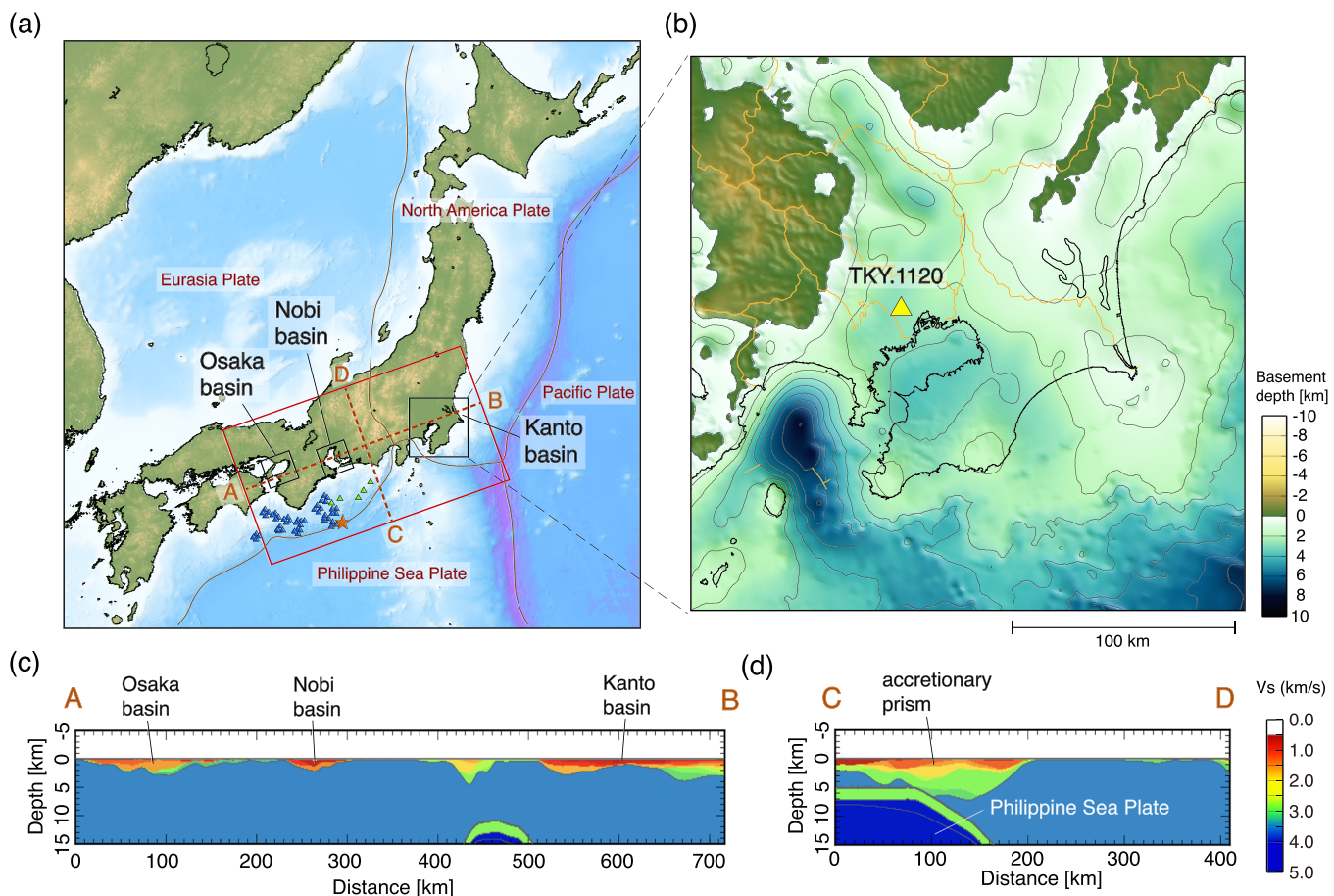


Figure 3. (a) Map showing the area of the data assimilation and forecast simulation of the LP ground motions (red rectangle). A red star represents the epicenter of the 2004 Off Kii Peninsula earthquake. Major large basins, such as the Kanto (Tokyo), Nobi, and Osaka basins, are indicated. Blue and green triangles denote the location of the DONET and JMA Cable OBS stations, respectively. (b) The basement depth (top of the $V_S = 2.7$ km/s layer) at the Kanto basin is shown along with the location of the SK-net station in Setagaya, Tokyo (TKY.1120; yellow triangle). (c) A vertical cross section along A–B and (d) C–D demonstrates thick sediments in large basins and in accretionary prism in the Nankai Trough subduction zone.

in the study of Cerjan et al. (1985) and a time increment of $\Delta t = 0.01$ s. The subsurface structural model of the crust and sedimentary layers was obtained from the Japan Seismic Hazard Information Station (J-SHIS) of the NIED (Fujiwara et al., 2006), and the model of the Philippine Sea plate is based on the JIVSM model (Koketsu et al., 2012). Deeper structures below the Moho are based on the ak135 standard Earth model (Kennett et al., 1995). Vertical cross sections of the simulation model (A–B in Figure 3c) demonstrate a cover of thick (3–4 km) sedimentary layers beneath the Osaka, Nobi, and Kanto basins, and Section C–D presents the distribution of low wave speed layers in the accretionary prism in the Nankai Trough (Figure 3d). With a minimum shear-wave velocity of 0.35 km/s and a grid size of 0.2 km, 3-D FDM simulation can calculate seismic waves in periods longer than 2.5 s, with a sampling of four grid points per minimum wavelength.

The weight matrix of the optimum interpolation operator is calculated assuming that the correlation of the seismic wavefield is described by a Gaussian distribution function with a correlation distance of 10 km, and the errors of the observed wavefield (σ_o) and forecasted wavefield (σ_b) are of the same order of magnitude ($\rho = \sigma_o/\sigma_b = 1.0$). The weight matrix is calculated in advance, and the same one is used throughout the data assimilation calculations.

The 3-D FDM simulation is conducted using the Oakforest-PACS supercomputer jointly operated by the Information Technology Center of the University of Tokyo and the University of Tsukuba. Through parallel computing using 2,048 CPUs, the wave propagation simulation of 100 s by 10,000 time step calculations took 42 s, that is, at the speed of 2.4 times faster than the actual wave propagation speed (see section S3).

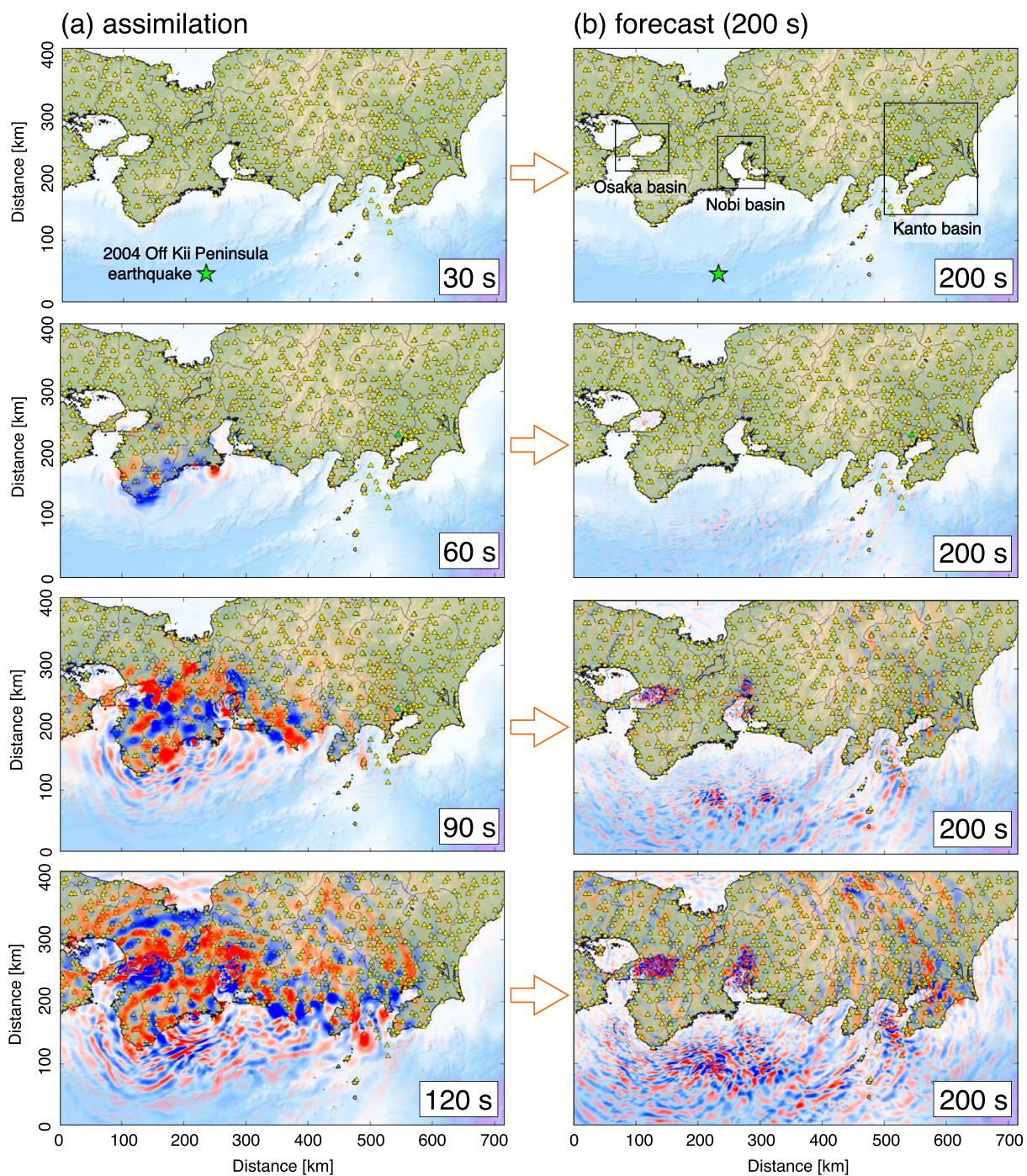


Figure 4. (a) Snapshots of the data assimilated wavefields of the N-S component ground velocity motions at 30, 60, 90, and 120 s from the earthquake origin time and (b) the forecasted future wavefields at 200 s obtained by forecast simulation from each assimilated wavefield being used as an initial conditions.

2.5. Results of the Forecast

Figure 4a presents the snapshots of the assimilated wavefield at 30, 60, 90, and 120 s from the earthquake occurrence time, obtained by the data assimilation between the observed ground motions at the K-NET and KiK-net stations and the simulated wavefield calculated by the 3-D FDM. The snapshots of the assimilated wavefield demonstrate the spread of ground motions from the source in the Nankai Trough to central Japan over time.

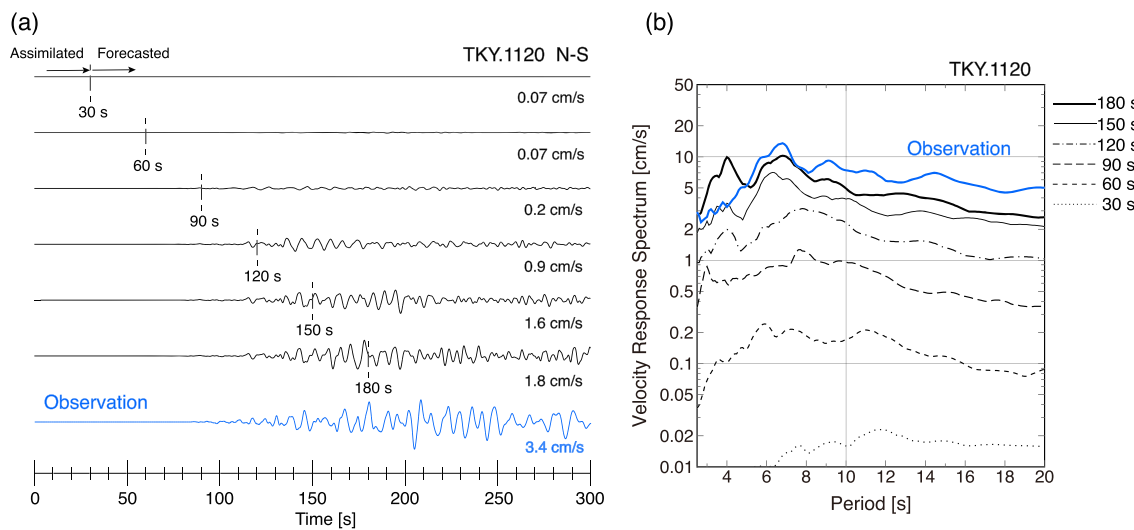


Figure 5. (a) A comparison is shown of the forecasted waveforms of the N-S component ground velocity (black lines) at the station TKY.1120 in Setagaya obtained by the forecast simulations from the assimilated wavefield at 30, 60, ..., 180 s from the earthquake occurrence time. The left and right segments of the vertical lines are the assimilated and forecasted waveforms, respectively. The observed waveform at this station is represented by the blue line. A band-pass filter (0.05–0.4 Hz) was applied, and the maximum amplitude of each trace is presented on the right. (b) The velocity response spectrum of the forecasted (black) and observed (blue) ground motions of horizontal components is presented with 5% damping.

Figure 4b shows the forecasted wavefields at 200 s obtained by the forecast simulation by 3-D FDM from each assimilated wavefield, demonstrating large and long-lasting shaking of LP ground motions is developed in large basins, such as the Osaka, Nobi, and Kanto basins. The forecasted wavefield from the assimilated wavefield at earlier times (30 s) is almost blank because large ground motions have not yet arrived at the K-NET and KiK-net stations on land. However, from 60 s subsequent to the earthquake occurrence time, when the ground motions arrive at the stations on land, the forecasted wavefields reveal large ground motions in basins. The amplitude of the forecasted LP wavefield increases steadily as the assimilation time progresses.

Figure 5a compares the forecasted waveforms of N-S component ground velocity at station TKY.1120 in Setagaya, Tokyo (Figure 3b) as a function of the data assimilation time of 30, 60, ..., 180 s with the observed waveform (bottom blue trace). Here we present the forecasted waveforms at this station where long-time recording was obtained, and the waveforms of other stations in the Kanto basin are shown in section S2. The observed waveform shows that the powerful LP ground motions started in Tokyo ~160 s after the earthquake occurrence time, then large ground motion continued for more than several hundred seconds. The forecasted waveforms shown in Figure 5a can be split into the two segments, the left and the right segments of the vertical line corresponds to the assimilated and forecasted waveform, respectively, on which the right segment of the waveforms should be focused. The results show that the forecast of the LP ground motions in Tokyo improved greatly as the data assimilation progressed with time. Also, the level of the forecast accuracy increased rapidly at 60 s from the earthquake occurrence time when large ground motions arrived at the K-NET and KiK-net stations on land.

In order to investigate the effects of the large-amplitude LP ground motions in Tokyo on the large-scale buildings, we calculated the response spectrum of the forecasted horizontal ground motions and compared them with the actual observations (Figure 5b). The forecast level of the velocity response in a period of 7 s, which was the dominant period of the LP ground motions in central Tokyo during this Mw 7.4 earthquake, increased gradually from 10% to 70% of the actual ground motions, with increasing data assimilation time from 90 to 180 s. The forecasted velocity response spectrum shows a slightly large amplitude around 4 s, although not in the observation. This is probably owing to the imperfection of the subsurface structure model used for the forecast simulations. As there is a large trade-off between the accuracy of the forecast and the lead time until strong LP ground motion starts in Tokyo, a repeated forecast, such as for every 5–10 s, may be necessary in conjunction with the acquisition of the strong motion data at the seismic network.

3. Faster Forecasting of LP Ground Motions Using Green's Functions

3.1. DAF With Green's Functions (DAF + G)

Modern high-performance computers with efficient parallel computing capabilities enable faster forecast simulations of seismic waves at speeds much faster than actual speed of surface waves. However, large-scale simulations including large source areas of the Nankai Trough earthquakes and the distant basins affected by the LP ground motions are still very expensive, particularly considering the need to repeat the forecast at short time intervals.

To realize much faster forecasting, we consider an another approach using precalculated Green's functions for wave propagation from the data assimilation stations to a forecast target site, instead of performing in situ 3-D FDM simulations of seismic wave propagation. Such a DAF using the Green's functions was first developed by Wang et al. (2017) for the early forecasting of tsunamis (GFTDA), and it was shown that this is equivalent to evaluating wave propagation by the FDM calculation. In seismology the term "Green's function" is formally defined as the response of displacement wavefield corresponding to a single force input (e.g., Aki & Richards, 2002); however, this study uses this term as the wave propagation response to a unit wavefield input (e.g., acceleration or velocity input at the data assimilation station).

By substituting Equation 1 of the forecasted wavefield into the assimilated wavefield Equation 3 recursively, the assimilated wavefield can be rewritten in the following form:

$$\mathbf{x}_n^a = \mathbf{F} \mathbf{x}_{n-1}^a + \mathbf{W} \mathbf{r}_n = \mathbf{F}^n (\mathbf{W} \mathbf{r}_0) + \mathbf{F}^{n-1} (\mathbf{W} \mathbf{r}_1) + \cdots + \mathbf{W} \mathbf{r}_n = \sum_{t=0}^n \mathbf{F}^{n-t} (\mathbf{W} \mathbf{r}_t) \quad (6)$$

with $\mathbf{r}_0 = \mathbf{y}_0$ because the forecasted wavefield is zero in the beginning ($\mathbf{x}_0^f = \mathbf{0}$).

We define the residual matrix at the time $t (=1, 2, \dots, n)$, \mathbf{r}_t , using the residual vector, \mathbf{r}_t^i at each station, i , and a unit vector, \mathbf{e}_i , as

$$\mathbf{r}_t = \sum_{i=1}^M \mathbf{e}_i (\mathbf{r}_t^i)^T \quad (7)$$

Then, substituting Equation 7 into Equation 6 gives

$$\mathbf{x}_n^a = \sum_{t=0}^n \mathbf{F}^{n-t} \left(\mathbf{W} \sum_{i=1}^M \mathbf{e}_i (\mathbf{r}_t^i)^T \right) = \sum_{i=1}^M \sum_{t=0}^n \mathbf{F}^{n-t} \mathbf{W} \mathbf{e}_i (\mathbf{r}_t^i)^T \quad (8)$$

Therefore, the forecast of the future wavefield after k time steps by 3-D FDM simulation can be obtained similarly by convolution of the residual at each data assimilation station, $\mathbf{e}_i (\mathbf{r}_t^i)^T$, and the Green's function of the wave propagation response, \mathbf{F}^t , from station i to j , multiplied by the weight matrix, \mathbf{W} , as

$$\mathbf{x}_{n+k}^f = \sum_{i=1}^M \sum_{t=0}^n \mathbf{F}^{n+k-t} \mathbf{W} \mathbf{e}_i (\mathbf{r}_t^i)^T \quad (9)$$

Hereafter, we call $\mathbf{W} \mathbf{e}_i$ the weighted Green's function, which describes the wave propagation response from i to j , multiplied by a spatially distributed weight of the optimum interpolation operator.

The weighted Green's functions are calculated in advance by 3-D FDM simulations, so that forecast of ground motions at the target site can be achieved instantaneously by convolving them with the residual at each data assimilation station (Figure 6), instead of running expensive 3-D FDM simulations in real time.

3.2. Calculation of Weighted Green's Functions Using the Reciprocity Theorem

The Green's function from data assimilation stations i to the forecast target sites j is calculated by loading a single unit wavefield given as the delta source time function at station i for each component $l (=x, y, z)$ (Figure 7a). The weighted Green's function can be obtained by summing up a set of Green's functions corresponding to the unit wavefield input on grids g around station i with weight W_{gi} (Figure 7b).

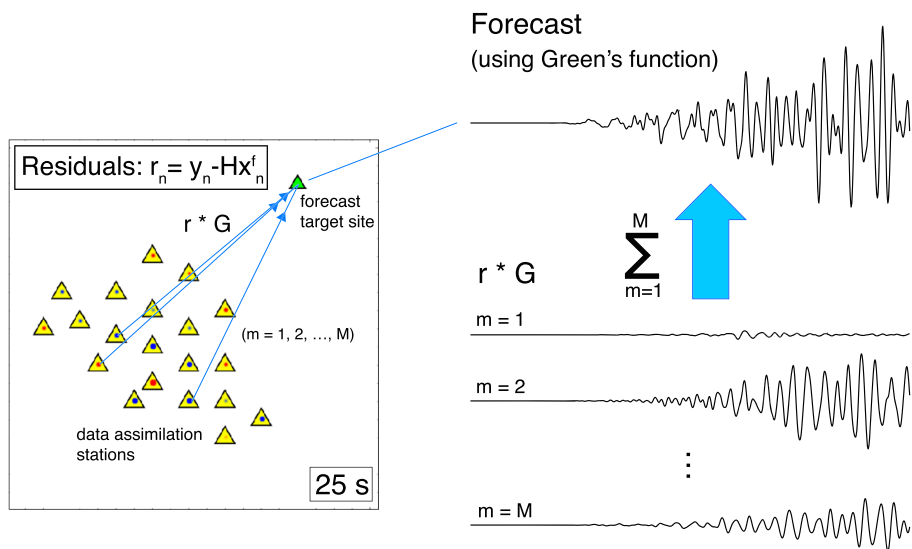


Figure 6. Schematic illustration of the DAF + G for instantaneous forecast of ground motion using precalculated Green's functions. The forecasted waveform at a target site is obtained through the convolution of the residual waveform at each data assimilation station with the weighted Green's functions that represents wave propagation from the data assimilation stations to the forecast target site, and then summing them up for all of the stations.

Here, the force vector, \mathbf{We}_i^l , of the weighted unit wavefield around i for component l is

$$\mathbf{We}_i^l = (W_{1i}, W_{2i}, \dots, W_{gi}, \dots, W_{Gi})^T \quad (10)$$

As the Green's function of the wave propagation response \mathbf{F} has the components $F_{jg}(x, y, z, t; x', y', z', t')$ hereafter referred as F_{jg}^{lm} ($m = x', y', z'$), which represents the response of component m at point j

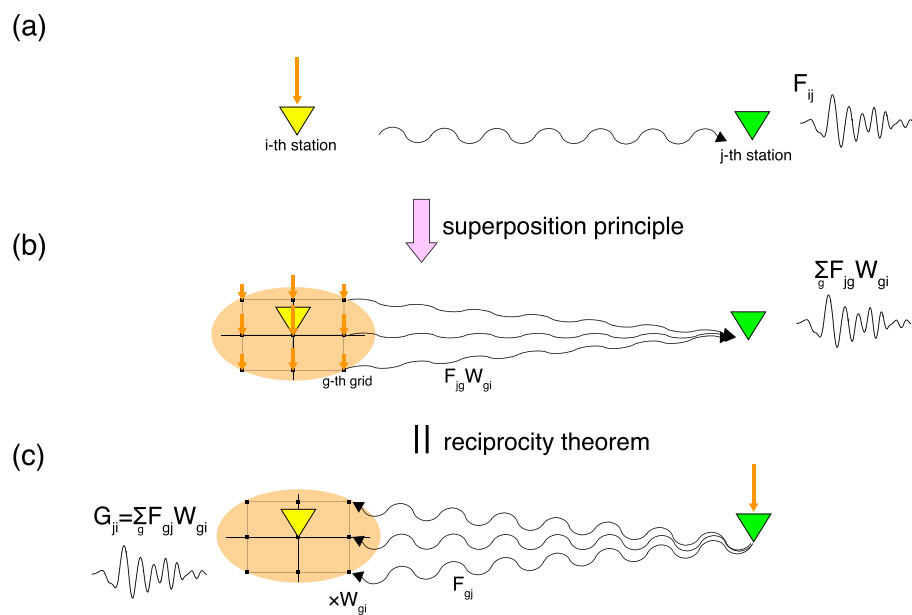


Figure 7. (a) Green's function of wave propagation response from i to j is obtained by FDM simulation with a single force at station i and examination of the response (waveform) at station j . (b) The weighted Green's function that corresponds to a set of weighted forces around i is obtained by using the superposition of the Green's function with the set of single forces at grid g ($=1,2,\dots,G$). (c) Using the reciprocity theorem, the weighted Green's function can be obtained effectively by exchanging i and j and summing up the response around i after weighting.

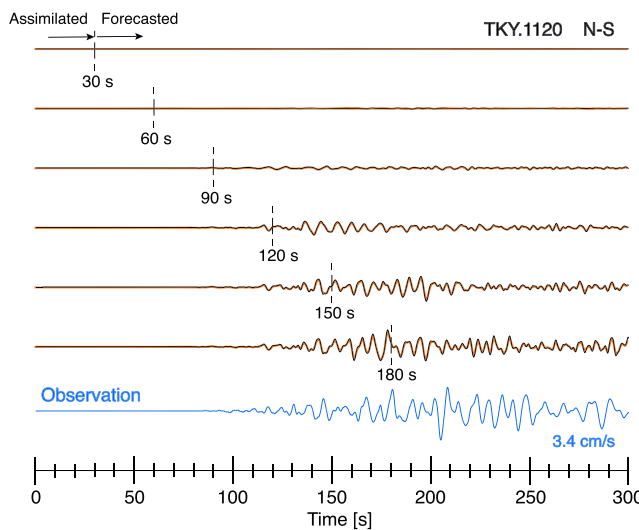


Figure 8. Comparison of the forecasted waveforms of the N-S component ground velocity at TKY.1120 as a function of the data assimilation time of 30, 60, ..., 180 s subsequent to the earthquake occurrence time as obtained by DAF (black line, same as in Figure 5a) and those obtained using the DAF + G (orange lines). The bottom blue trace represents observed ground motion from the 2004 Off Kii Peninsula earthquake. All traces are applied by a band-pass filter (0.05–0.4 Hz).

The waveform of the forecasted ground motion at station TKY.1120 in Setagaya, Tokyo, by DAF + G is presented in Figure 8 in orange traces, which is compared with the former forecast based on DAF (gray traces). Excellent agreement in the forecasted waveforms between the two schemes confirms the equivalence of the forecasting by using Green's function (DAF + G) and 3-D FDM simulation (DAF). A slight difference in the timing between the forecasted waveform occurs because the source time function used in the Green's function calculation is not exactly a delta function but has a finite duration (2.5 s) due to a requirement of the 3-D FDM simulation associated with the discretization.

Note that this DAF + G can forecast LP ground motions only for one target site, although not the entire simulation domain as performed by the DAF. The multipoint forecasts for large numbers of target sites require a large number of convolution calculations and may be less cost-effective than DAF. However, the forecast should be necessary only for a few target sites in the large basins, which have a high risk of LP ground motions, and moreover, the LP ground motions with longer wavelength do not need to be forecasted at dense intervals. Therefore, the DAF + G is a very effective approach for the early forecasting of LP ground motions in some large basins from distant large earthquakes.

4. Real-Time Forecasting of the LP Ground Motions for Large Nankai Trough Earthquakes

We applied the DAF + G for real-time forecasting of the LP ground motions for anticipated Nankai Trough earthquakes. The area of the numerical experiment is $1,228.8 \text{ km} \times 768.0 \text{ km}$ in horizontally and 100 km in vertically, which is discretized to 0.2 km grid spacing (Figure 9). In this experiment, data from the recently deployed DONET (Kawaguchi et al., 2008, 2015) and the JMA Cable ocean-bottom seismograph (Cable OBS; Saito, 2007) in the Nankai Trough (see Figure 9 for locations) were applied, in addition to the K-NET and KiK-net on land. Also, the N-net cable ocean-bottom stations, which are now being planned for installation in the west of the Nankai Trough (NIED, 2018), were applied. Such offshore stations in the Nankai Trough are expected to capture strong ground motions immediately after the occurrence of the earthquakes and will improve the data assimilation and forecasting of LP ground motions from an even earlier time. The total number of onshore and ocean bottom stations used for data assimilation is 1,229 (see Figure 9 for locations).

corresponding to the unit wavefield input of component l at point g . The component m of the weighted Green's functions $(\mathbf{FWe}_i^l)_j^m$ can be described as the superposition of the response, $F_{jg}^{lm}W_{gi}$, for a set of weighted unit wavefield inputs (Figure 7b) as:

$$(\mathbf{FWe}_i^l)_j^m = F_{j1}^{lm}W_{1i} + F_{j2}^{lm}W_{2i} + \dots + F_{jg}^{lm}W_{gi} + \dots + F_{jG}^{lm}W_{Gi} \quad (11)$$

In general, the total number of the forecast target sites is much smaller than the stations used for data assimilation; therefore, we use the reciprocity theorem to exchange g, j and l, m (e.g., Aki & Richards, 2002), then it can be expressed as

$$(\mathbf{FWe}_i^l)_j^m = F_{1j}^{ml}W_{1i} + F_{2j}^{ml}W_{2i} + \dots + F_{gj}^{ml}W_{gi} + \dots + F_{Gj}^{ml}W_{Gi} \quad (12)$$

The weighted Green's function can be then obtained very efficiently with a unit wavefield input on the forecast target site j ($\ll i$) to obtain waveforms at the grid points of the 3-D FDM simulation around the data assimilation station i , and then summing them up with the weights W_{gi} (Figure 7c).

3.3. Forecast of the LP Ground Motions by DAF + G

We applied the DAF + G for the forecast of the LP ground motions in Tokyo from the 2004 Off Kii Peninsula earthquake and compared these results with the forecast by the DAF presented in Figure 5.

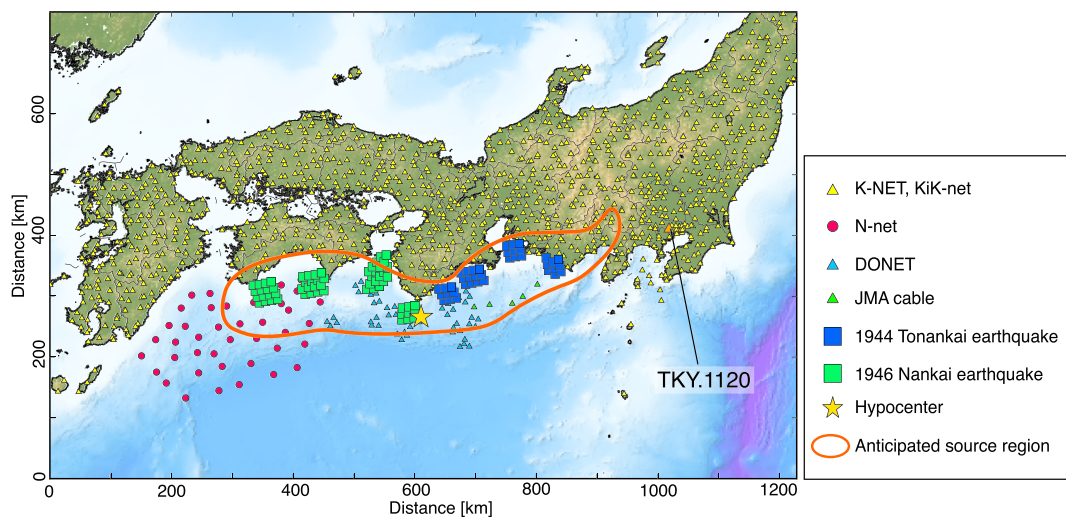


Figure 9. Area of the data assimilation and forecast of the LP ground motions for the Nankai Trough earthquakes. The source models of the 1944 Tonankai and the 1946 Nankai earthquake scenarios are represented by four segments of strong motion generation area (SMGA; green and blue patches), and a hypocenter is represented by a yellow star. The K-NET and KiK-net stations on land and the offshore DONET and the JMA Cable OBS stations are marked by triangles. The assumed location of the N-net stations (after NIED, 2018) is indicated by red circles. The forecast target site in Setagaya, Tokyo (TKY.1120), is marked by an orange triangle.

First calculated was the theoretical seismograms of the Nankai Trough earthquakes at each data assimilation station and a forecast target site, as an answer of the forecast experiment, using the source models of the 1944 Tonankai (Mw 7.9) and the 1946 Nankai (Mw 8.0) earthquakes for modeling of LP ground motions developed by the Cabinet Office of the Disaster Prevention Section (2015). Both source models consist of four segments of SMGAs (Figure 9), and fault ruptures run over the faults across the SMGAs from the hypocenter south of Off Kii Peninsula to the east and to the west for the 1944 and 1946 earthquake scenarios, respectively (Figure 9). Such fault rupture propagation over a large earthquake fault might have caused increased amplitude and duration of the LP ground motions. The synthetic seismograms of these Nankai Trough earthquake scenarios obtained by the 3-D FDM simulation and used as inputs for this test are presented in section S4. The effect of the low-wave speed sedimentary layers on the generation of LP ground motions is also shown in Figure S6.

4.1. Forecast of the LP Ground Motions for the 1946 Nankai Earthquake Scenario

The expected LP ground motions in Tokyo at station TKY.1120 for the 1946 Nankai earthquake scenario are presented in Figure 10a (bottom blue trace), demonstrating that a large ground shaking of more than 5 cm/s occurs about 180 s after the earthquake origin time, and then large and long-duration LP ground motions continued for several minutes. The significance of such large and long-duration LP ground motions developing in Tokyo was also demonstrated by the cumulative elastic energy of the horizontal ground motions, that is, the sum of the squares of ground velocity multiplied by half of the density (Figure 10b). The response spectrum of the synthesized ground motions, presented in Figure 10c, demonstrates that a large response of 80–100 cm/s occurs in periods of ~8–10 s, which was as large or larger than the level that collapsed the oil storage tank during the 2003 Off Tokachi earthquake (Mw 8.0) in Japan (Koketsu et al., 2009).

The results of the forecasted LP ground motions in Tokyo obtained by the DAF + G are presented in Figure 10a, and they are compared with the expected ground motions in Tokyo (bottom blue trace). The forecasted waveforms in Tokyo demonstrate good agreement between the expected LP ground motion in terms of amplitude, dominant period, and duration. The accuracy of the forecast increases steadily with the data assimilation time, especially after 50 s from the earthquake occurrence time when the fault rupture propagated over the second SMGA of the 1946 Nankai earthquake source model (section S4). Therefore, the early forecast of the LP ground motion in Tokyo can be performed at 50 s after the earthquake occurrence time with a good accuracy and a large lead time of more than 100 s before the large ground motion occurs.

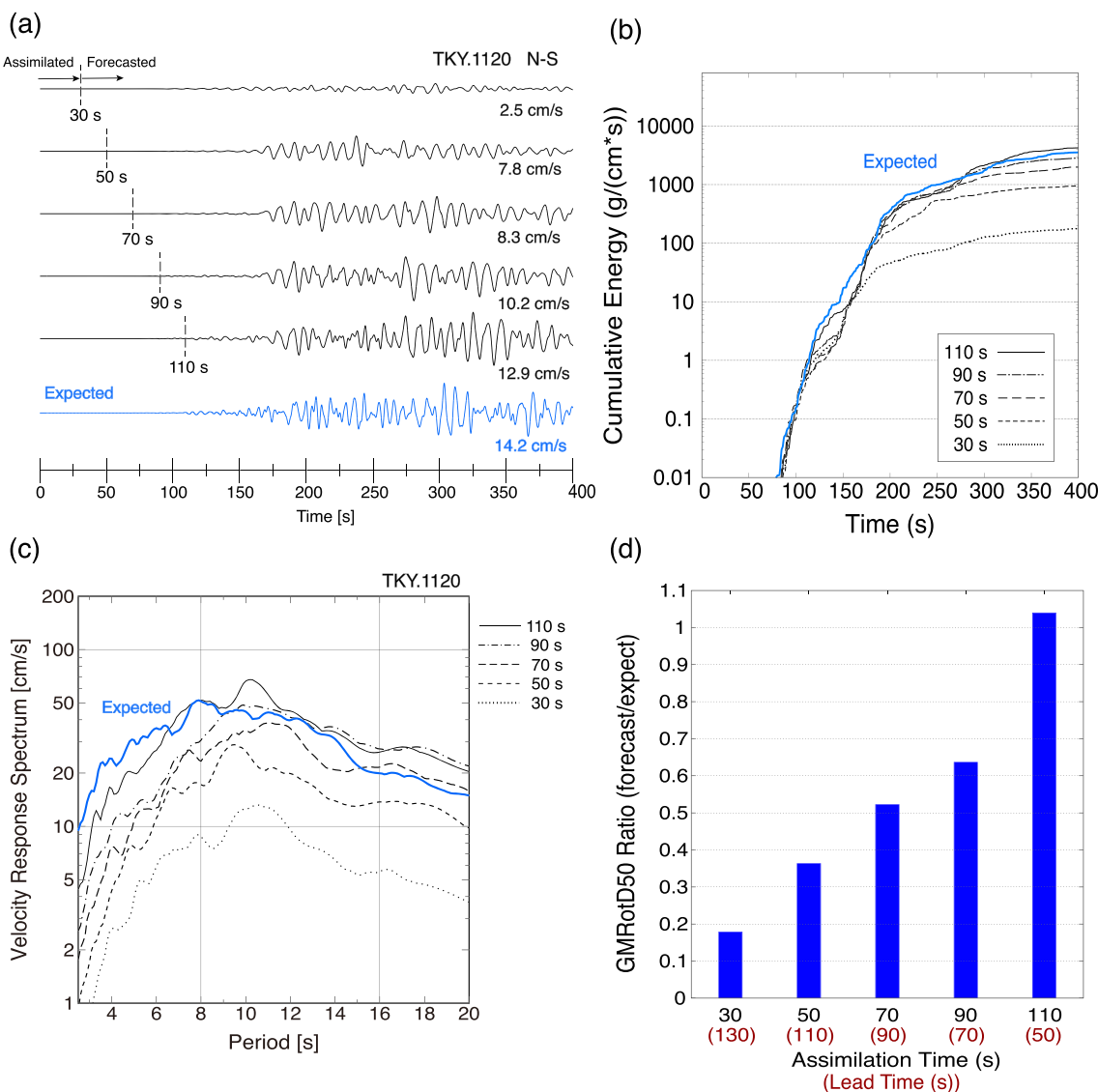


Figure 10. (a) Comparison of the forecasted waveforms of the N-S component ground velocity in Setagaya, Tokyo (TKY.1120), for the 1946 Nankai earthquake scenario (green squares in Figure 9) as a function of data assimilation time (30, 50, ..., 110 s) as compared with the expected ground motion (blue trace). All traces were applied by a band-pass filter (0.05–0.4 Hz), and a maximum amplitude is shown below. (b) Comparison of the cumulative elastic energy of each waveform is shown. (c) Velocity response spectra of the horizontal ground motions (5% dumping) as a function of data assimilation time and that of the expected ground motions are shown. (d) The ratio of the GMRotD50 (Boore et al., 2006) in period of 8 s relative to that of the expected ground motion is shown. The lead time is shown below each assimilation time, which was calculated by considering the arrival of large shaking in Tokyo as 160 s after the earthquake occurrence time.

To examine the increase in the forecast accuracy with data assimilation time, we calculated the GMRotD50 (Boore et al., 2006), the median velocity response spectra of horizontal components for a given period in rotating the orientation of horizontal components from 0° to 90° , for the forecasted waveforms at a period of 8 s. The GMRotD50 has recently been used to assess the strength of the ground motions independent of the direction of the epicenter (e.g., Barani et al., 2015; Imtiaz et al., 2015). The GMRotD50 ratio relative to that of the expected ground motion is shown in Figure 10d, confirming that the ratio increases gradually from 15% to 60% with increasing data assimilation time from 30 to 90 s. After 100 s, the GMRotD50 ratio increased suddenly to nearly 100% as the rupture of the earthquake fault plane had been completed (section S4 for snapshots of the seismic wave propagation).

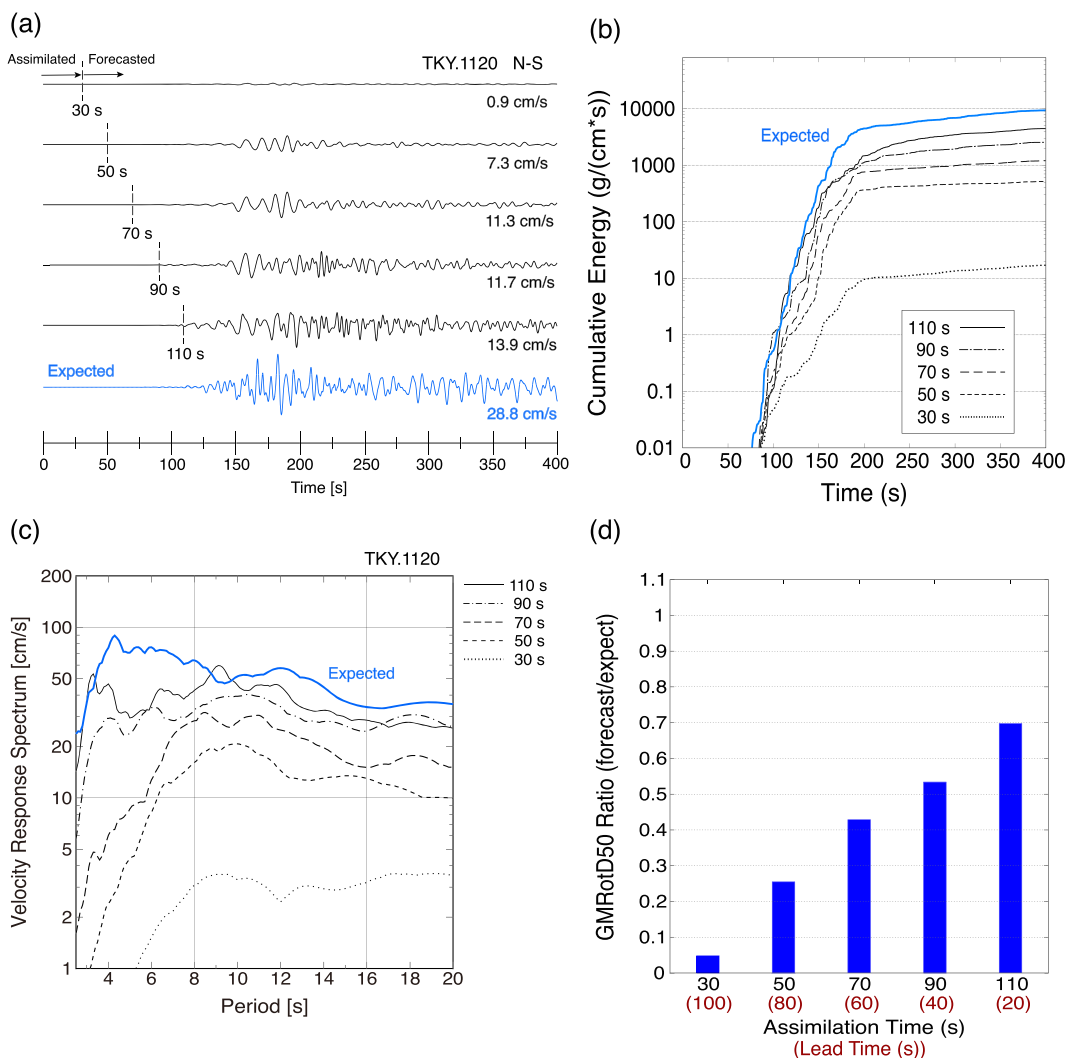


Figure 11. Same as Figure 10 but for the 1944 Tonankai earthquake scenario (blue squares in Figure 9). The lead time is calculated by considering the arrival of large shaking in Tokyo as 130 s after the earthquake occurrence time.

As the level of the forecast continues to grow with time as the fault rupture progresses over the large earthquake faults, the update of the forecast at short time intervals is necessary, along with the acquisition of the strong motion data.

4.2. Forecast of the LP Ground Motions for the 1944 Tonankai Earthquake Scenario

The early forecast of the LP ground motions was examined in an additional earthquake scenario, the 1944 Tonankai (Mw 7.9) earthquake. In this scenario, the fault rupture ran from the hypocenter in the south of the Off Kii Peninsula and east toward Tokyo, the opposite of the 1946 Nankai earthquake.

The results of the forecasted LP ground motions in Tokyo were compared in Figure 11 as a function of the data assimilation time with the expected ground motion. Compared with the former experiment for the 1946 Nankai earthquake scenario (Figure 9), the increase in the forecast accuracy over the time was much slower, especially before the assimilation time of 70 s. The growth of the response spectrum with time was also very gentle at 43% to 70% of the expected value with data assimilation time from 70 to 110 s. This occurred because the LP ground motions in Tokyo was mostly generated by the SMGA segment close to Tokyo (see Figure 9 for locations), which emitted large seismic waves after ~90 s of the earthquake occurrence time (snapshots of the seismic wave propagation are shown in section S4). Until these waves from the later

SMGA rupture were assimilated, the level of the forecasted LP ground motion in Tokyo continued to grow over time.

Therefore, for the forecasting of the LP ground motions from large earthquakes, care should be taken when the level of the forecast continues to increase while the forecast is updated, because this indicates a growth of the earthquake size. Therefore, the fast forecasting of LP ground motions through the use of DAF + G is very effective for repeating the forecast at short intervals as the assimilation progresses.

5. Discussion

In this study, the effectiveness of the DAF of LP ground motions was demonstrated using nationwide strong motion networks and fast computer simulations of seismic wave propagation. The effectiveness of the DAF was further improved using precalculated Green's functions (DAF + G) in order to accelerate the forecast calculations from the data assimilated wavefield.

5.1. Effectiveness of Offshore Cable Networks for Early Forecast

Recent developments of offshore cable ocean-bottom seismic networks in the Nankai Trough, such as the DONET and the JMA Cable OBS, are expected to play an important role in the early forecasting of LP ground motions from the Nankai Trough earthquakes, as they can capture the spread of ground motions above the source region soon after the occurrence of earthquakes.

To demonstrate the significance of such offshore networks for the early forecast of LP ground motions, a numerical test was performed using synthetic seismograms of the 2004 Off Kii Peninsula earthquake for the offshore DONET and JMA Cable OBS stations, as well as the K-NET and KiK-net stations on land. The synthetic seismograms of this earthquake were calculated by a 3-D FDM simulations with a double-couple point source of the F-net CMT focal mechanism (strike = 245°, dip = 62°, rake = 62°, depth = 11 km) and a 15 s t-exponential source time function. Synthetic records were utilized in this test because no large ($M_w > 7$) earthquakes have occurred since the deployment of these offshore stations. The synthetic seismograms for the offshore stations are presented in section S5.

The results of the forecasted ground motions by DAF + G at station TKY.1120 in Setagaya using the offshore stations records are presented in Figure 12a, demonstrating the significant improvements in forecasting, even from shorter data assimilation times (<30 s) as compared with that by using only the onshore stations (Figure 12b). Also, the response spectrum of the forecasted LP ground motions becomes much closer to that of the expected ground motions even from earlier assimilation times.

Without using the offshore stations, the forecast was largely underestimated, as ground motions took approximately 60 s to reach the data assimilation stations on land more than 100 km from the hypocenter (Figure 4a). In addition, the use of offshore stations above the source is also very effective for capturing the spread of the wavefronts radiated from the source in all directions, while the azimuthal range of land stations is relatively small.

5.2. Effect of Imperfections of the Subsurface Structure Model on the Data Assimilation and Forecast

The J-SHIS subsurface structure model used for the data assimilation and forecasting by 3-D FDM simulation was constructed based on a large number of reflection and refraction experiments, and the analysis of microtremors and other studies (Fujiwara et al., 2006). However, owing to the limited offshore exploration data, considerable uncertainties in the model are expected in the sea area.

To examine the effects of possible imperfections in the subsurface structure model in the sea area on data assimilation and forecasting, a numerical test was performed using inconsistent models in making the input waveforms and assimilation and forecasting. For this test, a modified J-SHIS model was created by excluding a low-velocity ($V_s \leq 1.0$ km/s) layer at the top of the accretionary prism in the Nankai Trough, while the synthetic seismograms for the 2004 Off Kii Peninsula earthquake, used for input motions of the data assimilation, were calculated using the unmodified J-SHIS model.

The results of the forecasted ground motions in Tokyo using the inconsistent structure model are presented in Figure 13a, which are compared with the results using the consistent model (Figure 12a). With the

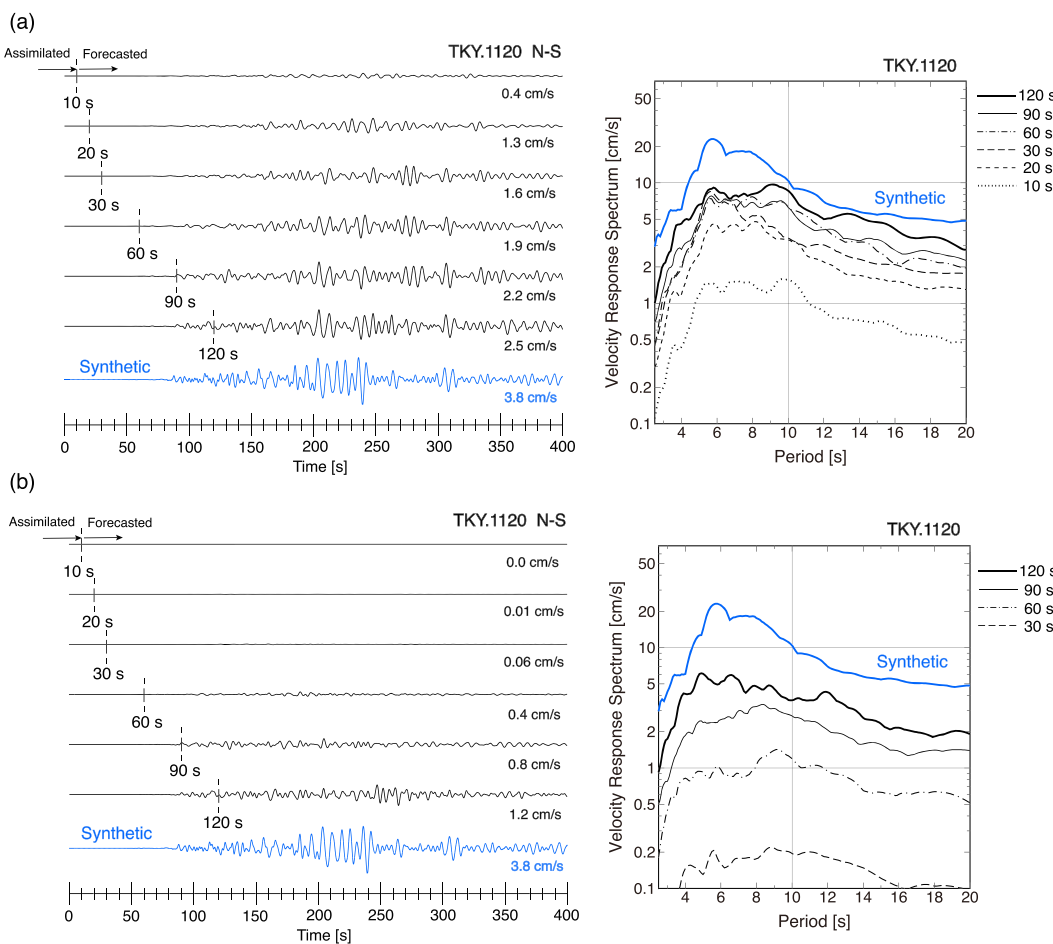


Figure 12. Comparison of the forecasted waveform of the N-S component ground velocity and the response spectrum of horizontal ground motions at TKY.1120 in Setagaya as a function of data assimilation time at 10, 20, ..., 120 s subsequent to the earthquake occurrence time. This experiment used synthetic seismograms from the 2004 Off Kii Peninsula earthquake. The expected ground motion is indicated by the bottom blue trace. (a) using the offshore DONET and JMA Cable OBS stations (see Figure 3 for locations) together with the K-NET and KiK-net stations on land. (b) Using only K-NET and KiK-net stations. All the waveforms were applied by a band-pass filter (0.05–0.4 Hz).

improper structure model in the data assimilation and forecasting, the amplitude of the forecasted waveform largely underestimated the expected ground motions, especially around 200 s after the earthquake occurrence time. Such underestimation in the forecasted LP ground motion was also confirmed in the response spectrum in periods of ~ 6 s. This means that the simulated wavefield has not been sufficiently corrected by the assimilation with the observation data in the sea area.

To minimize the effects of the possible model imperfections in the sea area on assimilation and forecasting, we changed the weight of the optimum interpolation operator between the offshore DONET and JMA Cable OBS stations and the other stations on land. The weight matrix was calculated, assuming a larger error in the simulated wavefield than the observation error ($\rho_i = 0.2$) for the offshore stations. The weights for the K-NET and KiK-net stations on land were calculated, assuming that the subsurface structure model of the land area was reliable and the error between simulation and observation was the same level ($\rho_i = 1.0$).

The results with the modified weight matrix are presented in Figure 13b, demonstrating fairly good improvement in the forecasting of LP ground motions in Tokyo along with a better fit between forecasted waveform and expected ground motions, compared with the former results (Figure 13a) assuming a uniform weight ($\rho_i = 1.0$) for all the stations.

Here we considered the effect of the simulation error caused by the imperfections of the subsurface structural model, particularly in the sea area; however, it may also need to be considered the errors associated

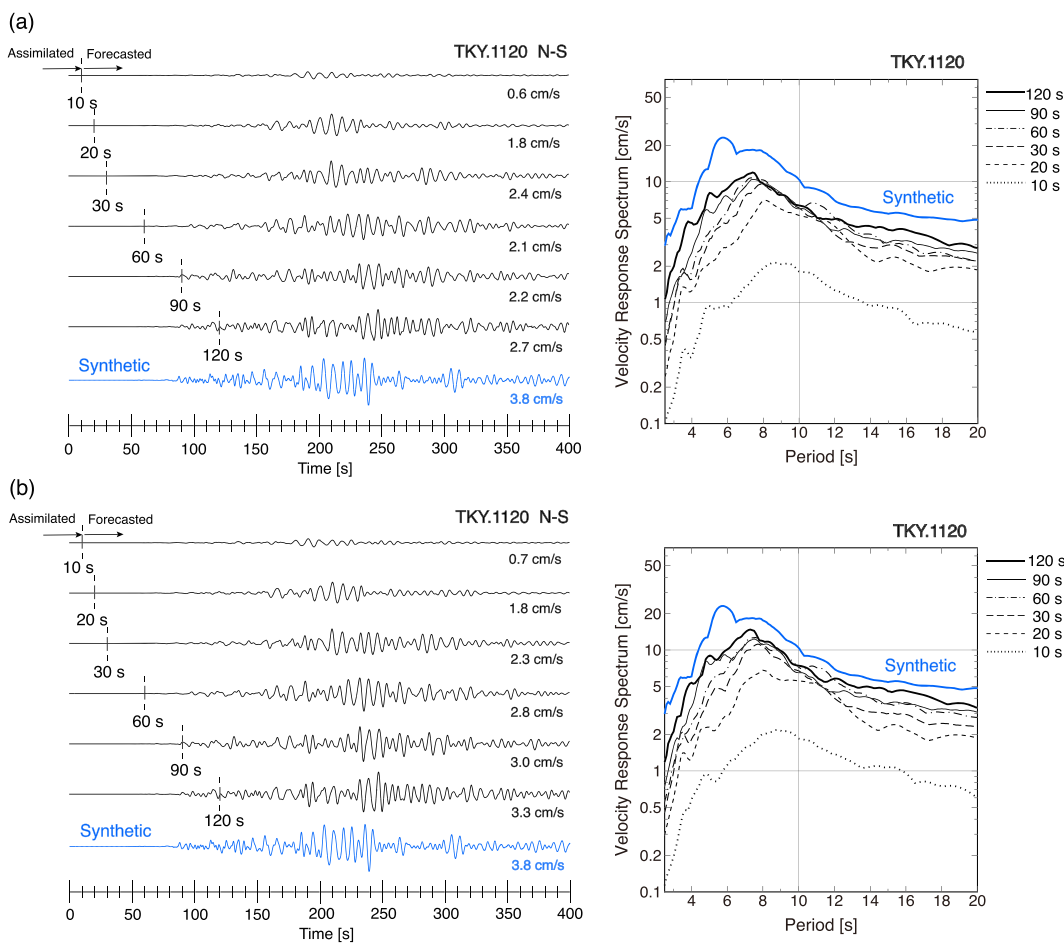


Figure 13. (a) The results of the forecasted waveforms in Setagaya (TKY.1120) and the velocity response spectrum obtained using the “inconsistent” model for the data assimilation and forecasting are compared with the expected ground motions (bottom blue trace). The optimum interpolation data assimilation parameters of $\rho_i = 1.0$ are used for all the stations. (b) The results of the forecast using $\rho_i = 0.2$ for the offshore DONET and JMA Cable OBS stations, and $\rho_i = 1.0$ for the K-NET and KiK-net stations on land. All the waveforms are applied by a band-pass filter (0.05–0.4 Hz).

with observations, such as occurred by nonlinear soil response owing to large ground motions, large noise at the sea bottom such as caused by strong ocean current, and the defects in observation sensors, and so on when utilizing the real data from offshore stations.

6. Conclusions

In order to mitigate LP ground motion hazards caused by large earthquakes along the Nankai Trough, an early forecast of the LP ground motions based on the data assimilation of the observed ground motions by nationwide networks and the fast 3-D FDM simulations of seismic waves using a high-performance supercomputer was applied. In this study, it was also demonstrated that the speed of the forecast can be improved significantly by using precalculated Green’s functions corresponding to the wave propagation response from the data assimilation stations to the forecast target site, instead of conducting in situ 3-D FDM simulations.

If the forecast of the LP ground motions with sufficient lead time is achieved, it is expected that actions can be taken to mitigate the damage caused by the LP ground motions, such as stopping elevators of skyscrapers safely, alerting occupants of buildings to cope with large and long-time shaking, and clarifying the possible building damage to assess the need for evacuation.

The effectiveness of this DAF + G-based early forecasting of LP ground motions in Tokyo from the Nankai Trough earthquakes was demonstrated by numerical experiments using the observed waveform data from

the 2004 Off Kii Peninsula earthquake (Mw 7.4) and synthetic seismograms of anticipated Nankai Trough earthquake scenarios. The results confirmed that the alert of the LP ground motions in Tokyo could be issued with sufficient lead time of several tens of seconds before a strong shaking occurs.

The results of this study also confirmed the effectiveness of the recently deployed ocean-bottom cable network in the Nankai Trough to increase the accuracy and lead time for the forecast, as they detect ground motions immediately after the occurrence of large earthquakes and capture the spread of wave-front in all directions from the source. To make the best use of the offshore observations, assimilation must be conducted taking into account relatively large errors in both the calculation results and the observation data.

Data Availability Statement

The K-NET and KiK-net (<https://doi.org/10.17598/NIED.0004>) strong motion records used in this study are available at the NIED webpage (<http://www.seis.bosai.go.jp>). The SK-net records are available online (at <http://www.sknet.eri.u-tokyo.ac.jp>). The J-SHIS model can be downloaded from the Japan Seismic Hazard Station website (at <http://www.j-shis.bosai.go.jp/en/downloads/>), and the JIVSM model can be downloaded from the webpage of the Headquarters for Earthquake Research Promotion (at https://www.jishin.go.jp/evaluation/seismic_hazard_map/lphsm/12_choshuki_dat/). The Nankai Trough earthquake source model from the Cabinet Office of the Disaster Prevention Section (2015) is available from the database of the Association for Promotion of Infrastructure Geospatial Information Distribution (https://www.geospatial.jp/gp_front/). A code for calculating the weight matrix of the optimum interpolation can be found at GitHub (<https://github.com/tktmyd/tdac>), and this was used together with the tsunami data assimilation model (Maeda et al., 2015). The source codes for the seismic wave propagation simulations (OpenSWPC; Maeda et al., 2017) are available at GitHub (<https://github.com/tktmyd/OpenSWPC>). The input parameter files for the 3-D FDM simulation of the 1946 Nankai and 1944 Tonankai earthquakes are uploaded to GitHub, and they can be accessed online (at <https://zenodo.org/badge/latestdoi/238653003>).

Acknowledgments

We thank two anonymous reviewers and the editor of JGR-Solid Earth Martha Savage for their careful reading and constructive comments that greatly improved the manuscript. This study was supported by Grants-in-Aid from the Japan Society of Promotion Sciences (17K01322). The TM was supported by Grants-in-Aid from the Japan Society of Promotion Sciences (19K04006) and by the JST CREST Project (JPMJCR1763). The computations were conducted using the Earth Simulator at Japan Marine Science and Technology Center (JAMSTEC), Orkforest-PACS computer, jointly operated by the Supercomputer Center of the University of Tokyo and the University of Tsukuba and the EIC parallel computer at the Earthquake Information Center at the Earthquake Research Institute of the University of Tokyo.

References

- Aki, K., & Richards, P. G. (2002). *Quantitative seismology*, (2nd ed.). Sausalito: University Science Books.
- Ando, M. (1975). Source mechanisms and tectonic significance of historical earthquakes along the Nankai Trough, Japan. *Tectonophysics*, 27(2), 119–140. [https://doi.org/10.1016/0040-1951\(75\)90102-X](https://doi.org/10.1016/0040-1951(75)90102-X)
- Aoi, S., Kunugi, T., Nakamura, H., & Fujiwara, H. (2011). Deployment of new strong motion seismographs of K-NET and KiK-net. *Earthquake data in engineering seismology* (Vol. 14, pp. 167–186). Dordrecht: Springer. https://doi.org/10.1007/978-94-007-0152-6_12
- Asano, K., & Iwata, T. (2012). Source model for strong ground motion generation in the frequency range 0.1–10 Hz during the 2011 Tohoku earthquake. *Earth, Planets and Space*, 64(12), 1111–1123. <https://doi.org/10.5047/eps.2012.05.003>
- Barani, S., Albarello, D., Spallarossa, D., & Massa, M. (2015). On the influence of horizontal ground shaking definition on probabilistic seismic-hazard analysis. *Bulletin of the Seismological Society of America*, 105(5), 2704–2712. <https://doi.org/10.1785/0120150033>
- Beck, J. L., & Hall, J. F. (1986). Factors contributing to the catastrophe in Mexico City during the earthquake of September 19, 1985. *Geophysical Research Letters*, 13(6), 593–596. <https://doi.org/10.1029/GL013i006p00593>
- Blanch, J. O., Robertsson, J. O. A., & Symes, W. W. (1995). Modeling of a constant Q: Methodology and algorithm for an efficient and optimally inexpensive viscoelastic technique. *Geophysics*, 60(1), 176–184. <https://doi.org/10.1190/1.1443744>
- Boore, D. M., Watson-Lamprey, J., & Abrahamson, N. A. (2006). Orientation-independent measures of ground motion. *Bulletin of the Seismological Society of America*, 96(4A), 1502–1511. <https://doi.org/10.1785/0120050209>
- Cabinet Office (2015). Source models of great subduction-zone earthquakes along the Nankai trough. http://www.bousai.go.jp/jishin/nankai/nankaitrough_report.html [in Japanese].
- Cerjan, C., Kosloff, D., Kosloff, R., & Reshef, M. (1985). A nonreflecting boundary condition for discrete acoustic and elastic wave equations. *Geophysics*, 50(4), 705–708. <https://doi.org/10.1190/1.1441945>
- Denolle, M. A., Dunham, E. M., Prieto, G. A., & Beroza, G. C. (2013). Ground motion prediction of realistic earthquake sources using the ambient seismic field. *Journal of Geophysical Research: Solid Earth*, 50, 705–708. <https://doi.org/10.1029/2012JB009603>
- Dhakal, Y. P., Suzuki, W., Kunugi, T., & Aoi, S. (2015). Ground motion prediction equations for absolute velocity response spectra (1–10 s) in Japan for earthquake early warning. *Journal of Japan Association for Earthquake Engineering*, 15(6), 6_91–6_111. https://doi.org/10.5610/jaae.15.6_91
- Frankel, A., Wirth, E., Marafi, N., Vidale, J., & Stephenson, W. (2018). Broadband synthetic seismograms for magnitude 9 earthquakes on the Cascadia megathrust based on 3D simulations and stochastic synthetics, Part 1. Methodology and overall results. *Bulletin of the Seismological Society of America*, 108(5A), 2347–2369. <https://doi.org/10.1785/0120180034>
- Fujiwara, H., S. Kawai, S. Aoi, T. Ishii, T. Okumura, Y. Hayakawa, et al., (2006). Japan Seismic Hazard Information Station, J-SHIS, Proceedings of 8th US National Conference on Earthquake Engineering; Paper 554.
- Furumura, T. (2014). Risk of long-period ground motion due to the deep basement structure of the Kanto basin [in Japanese with English abstracts]. *Journal of Geography*, 123(5), 234–450.
- Furumura, T., & Hayakawa, T. (2007). Anomalous propagation of long-period ground motions recorded in Tokyo during the 23 October 2004 Mw 6.6 Niigata-ken Chuetsu, Japan, earthquake. *Bulletin of the Seismological Society of America*, 97(3), 863–880. <https://doi.org/10.1785/0120060166>

- Furumura, T., Hayakawa, T., Nakamura, M., Koketsu, K., & Baba, T. (2008). Development of long-period ground motions from the Nankai trough, Japan, earthquake: Observations and computer simulation of the 1944 Tonankai (mw 8.1) and the 2004 SE Off-Kii Peninsula (Mw 7.4) earthquakes. *Pure appl. Geophysics*, 165, 585–607. https://doi.org/10.1007/978-3-7643-8757-0_8
- Furumura, T., Maeda, T., & Oba, A. (2019). Early forecast of long-period ground motions via data assimilation of observed ground motions and wave propagation simulations. *Geophysical Research Letters*, 46, 138–147. <https://doi.org/10.1029/2018GL081163>
- Furumura, T., & Nakamura, M. (2006). Recovering of strong motion record of the 1944 Tonankai earthquake and long period ground motion in Kanto region [in Japanese with English abstracts]. *Butsuri-Tansa*, 59, 337–351.
- Hatayama, K., & Zama, S. (2005). Sloshing of liquid in oil storage tanks and long-period strong ground motions due to 2004 M7-class earthquakes southeast off the Kii Peninsula [in Japanese]. *Report of National Research Institute of Fire and Disaster*, 99, 52–67.
- Hayakawa, T., Furumura, T., & Yamanaka, Y. (2005). Simulation of strong ground motions caused by the 2004 off the Kii peninsula earthquakes. *Earth, Planets and Space*, 57(3), 191–196. <https://doi.org/10.1186/BF03351814>
- Headquarters for Earthquake Research Promotion (2018). Evaluation of occurrence potentials or subduction-zone earthquake. https://www.jishin.go.jp/evaluation/long_term_evaluation/chousa_18feb_kakuritsu_index/
- Hoshiba, M., & Aoki, S. (2015). Numerical shake prediction for earthquake early warning: Data assimilation, real-time shake mapping, and simulation of wave propagation. *Bulletin of the Seismological Society of America*, 105(3), 1324–1338. <https://doi.org/10.1785/0120140280>
- Ibrahim, R., Si, H., Koketsu, K., & Miyake, H. (2016). Long-period ground motion prediction equations for moment magnitude estimation of large earthquakes in Japan. *Bulletin of the Seismological Society of America*, 106(1), 54–72. <https://doi.org/10.1785/0120140244>
- Imtiaz, A., Causse, M., Chaljub, E., & Cotton, F. (2015). Is ground-motion variability distance dependent? Insight from finite-source rupture simulations. *Bulletin of the Seismological Society of America*, 105(2A), 950–962. <https://doi.org/10.1785/0120140107>
- Kalnay, E. (2003). *Atmospheric modeling, data assimilation, and predictability*. Cambridge: Cambridge University Press.
- Kawabe, H., & Kamae, K. (2013). Source modeling of the 2011 Off the Pacific Coast of Tohoku earthquake. *Journal of Japan Association for Earthquake*, 13(2), 75–87.
- Kawaguchi, K., Y. Kaneda, and E. Araki, (2008). The DONET: A real-time seafloor research infrastructure for the precise earthquake and tsunami monitoring. OCEANS 2008: MTS/IEEE Kobe Techno-Ocean, Kobe, Japan, April 8–11.
- Kawaguchi, K., Kaneko, S., Nishida, T., & Komine, T. (2015). Construction of the DONET real-time seafloor observatory for earthquakes and tsunami monitoring. In *SEAFLOOR OBSEVATORIES* (pp. 211–228). Berlin Heidelberg: Springer. https://doi.org/10.1007/978-3-642-11374-1_10
- Kennett, B., Engdahl, R., & Buland, R. (1995). Constraints on seismic velocities in the Earth from traveltimes. *Geophysical Journal International*, 122(1), 108–124. <https://doi.org/10.1111/j.1365-246X.1995.tb03540.x>
- Koketsu, K., Hatayama, K., Furumura, T., Ikegami, Y., & Akiyama, S. (2009). Damaging long-period ground motions from the 2003 Mw 8.3 Tokachi-oki, Japan earthquake. *Seismological Research Letters*, 76(1), 67–73. <https://doi.org/10.1785/gssrl.76.1.67>
- Koketsu, K., H. Miyake, and H. Suzuki, (2012). Japan integrated velocity structure model Version 1. In: Proceedings of 15th WCEE:1773.
- Kurahashi, S., & Irikura, K. (2013). Short-period source model of the 2011 Mw 9.0 Off the Pacific coast of Tohoku earthquake. *Bulletin of the Seismological Society of America*, 103(2B), 1373–1393. <https://doi.org/10.1785/0120120157>
- Maeda, T., Obara, K., Shinohara, M., Kanazawa, T., & Uehira, K. (2015). Successive estimation of a tsunami wavefield without earthquake source data: A data assimilation approach toward real-time tsunami forecasting. *Geophysical Research Letters*, 42, 7923–7932. <https://doi.org/10.1002/2015GL065588>
- Maeda, T., Takemura, S., & Furumura, T. (2017). OpenSWPC: An open-source integrated parallel simulation code for modelling seismic wave propagation in 3D heterogeneous viscoelastic media. *Earth and Planetary Science Letters*, 69(1), 102. <https://doi.org/10.1186/s40623-017-0687-2>
- Miyake, H., & Koketsu, K. (2005). Long-period ground motions from a large offshore earthquake: The case of the 2004 off the Kii peninsula earthquake, Japan. *Earth, Planets and Space*, 57(3), 203–207. <https://doi.org/10.1186/BF03351816>
- Mukai, Y., Furumura, T., & Maeda, T. (2018). Causes of azimuthally dependent amplification variations of long-period ground motions in the Kanto basin, Central Japan [in Japanese with English abstracts]. *Bulletin of the Earthquake Research Institute*, 93, 31–48.
- National Research Institute for Earth Science and Disaster Resilience (2018). Plan of construction of the ocean floor earthquake and tsunami monitoring network around the Nankai trough region; N-net. http://www.mext.go.jp/component/a_menu/science/detail/_icsFiles/afieldfile/2019/03/11/1285826_02.pdf [in Japanese].
- Saito, S. (2007). JMA's new ocean bottom seismographs (OBS) using marine cable installed at the Sea of Enshu to the Sea of Kumano. *Chikyu Mon*, 29, 516–522.
- Uetake, T. (2017). Effects of subsurface structures of source regions on long-period ground motions observed in the Tokyo Bay area, Japan. *Earth, Planets and Space*, 69(1), 71. <https://doi.org/10.1186/s40623-017-0655-x>
- Wang, Y., Satake, K., Maeda, T., & Gusman, A. R. (2017). Green's function-based tsunami data assimilation: A fast data assimilation approach toward tsunami early warning. *Geophysical Research Letters*, 44, 10,282–10,289. <https://doi.org/10.1002/2017GL075307>
- Wirth, E. A., Vidale, J. E., Frankel, A. D., Pratt, T. L., Marafi, N. A., Thompson, M., & Stephenson, J. (2019). Source-dependent amplification of earthquake ground motions in deep sedimentary basins. *Geophysical Research Letters*, 46, 6443–6450. <https://doi.org/10.1029/2019GL082474>
- Yokota, Y., Ikeuchi, K., Yahagi, T., Kaida, Y., & Suzuki, H. (2011). Attenuation and amplification of long-period component of ground motion [in Japanese with English abstracts]. *Journal of Japan Association for Earthquake*, 11(1), 81–101.
- Yuzawa, Y., & Kudo, K. (2011). Empirical predictive model for long-period (1–15 s) ground motion on hard rocks. *Journal of Structural and Construction Engineering*, 76, 519–526.
- Yuzawa, Y., & Nagumo, H. (2012). Factors of variability and measures for the shakeability of long-period ground motion—Kanto basin as an example [in Japanese with English abstracts]. *Journal of Japan Association for Earthquake*, 12(2), 41–59.